

Parameter and Index Images of Benzodiazepine Receptor Concentration in the Brain

Philippe Millet, Jacques Delforge, François Mauguier, Sabina Pappata, Luc Cinotti, Vincent Frouin, Yves Samson, Bernard Bendriem and André Syrota

CERMEP, Centre d'Exploration et de Recherche par Emission de Positons, Lyon, France; and CEA, INSERM U334, Service Hospitalier Frédéric Joliot, Commissariat à l'Énergie Atomique, Orsay, France

In vivo studies of ligand-receptor interactions with PET data are based on different approaches that provide either quantitative results (receptor density and affinity) or indices that are assumed to be correlated with the receptor concentration. The aims of this study are to obtain parametric images of benzodiazepine receptor concentration and of flumazenil affinity and to study the validity of two receptor concentration indexes. **Methods:** A three-compartment ligand-receptor model, [^{11}C]flumazenil, and experimental data obtained using a three-injection protocol in human volunteers were used to acquire parametric images. The delayed activity method and the apparent distribution volume (estimated using a two-compartment model) were also tested and their results compared with those of the multi-injection approach. **Results:** Parametric images of receptor density, affinity and all kinetic parameters were obtained with acceptable variation coefficients. A correlation between receptor density and apparent affinity was found ($r = 0.83$; $p < 0.0005$). The correlation between receptor concentration and apparent distribution volume (estimated with three- and two-compartment models, respectively) was assessed using both a linear (the usual hypothesis) and a nonlinear correlation derived from the relationship between the receptor density and the affinity. **Conclusion:** In spite of the complexity of this protocol (three injections, a 2-hr experiment, blood sampling and a metabolite study), we showed that the multi-injection approach is suitable for parametric brain imaging. By using this approach as a reference, we deduced that the distribution volume and delayed activity images are valid methods in the usual range of the benzodiazepine receptor concentrations found in the human brain.

Key Words: parametric imaging; benzodiazepine receptors; carbon-11-flumazenil; positron emission tomography; compartmental modeling; brain

J Nucl Med 1995; 36:1462–1471

Benzodiazepine receptors have been studied in humans using PET and [^{11}C]flumazenil ([^{11}C]FMZ), an antagonist ligand with high affinity and selectivity for central benzo-

diazepine receptors (1–3). Recent developments in mathematical compartmental analysis have enabled quantification of receptor concentration and ligand affinity of these receptors in the human brain. All previously described methods, however, are based on the ligand-receptor interaction model, whose usual structure includes three compartments (plasma, free and bound ligand) and five parameters (the receptor concentration, B'_{max} , and four kinetic parameters, including association and dissociation rate constants). The typical approach is to perform a kinetic PET experiment, define regions of interest (ROIs) on brain activity maps and deduce the corresponding time-concentration curves. Depending on the modeling approach implemented, these curves are used in one of three ways:

1. To calculate an index that presumably correlates with the receptor concentration [e.g., the distribution volume approach proposed by Koeppe et al. (4)].
2. To estimate receptor concentration directly [e.g., the equilibrium approach based on Scatchard analysis (5)].
3. To estimate ligand-receptor interaction model parameters by using a fitting procedure, which may or may not include receptor concentration.

Although the PET data correspond to ligand concentration images, model parametric estimates are usually obtained only for a few ROIs. Therefore, methods have been devised to obtain parametric images of the receptor concentration and some kinetic parameters. The advantage of such images is visual screening of ligand transport and receptor site concentration in the entire brain. Similar to the ROI approach, these imaging methods can provide receptor concentration images directly or index images of receptor concentration. In the latter case, the correlation between these indices and the receptor concentration requires validation studies.

The easiest approach assumes that the regional ligand concentration images obtained approximately 20 min after injection of [^{11}C]flumazenil reflect benzodiazepine receptor density (6). The main advantage of this approach is its simplicity. Koeppe et al. (4) have suggested the use of a two-parameter, two-compartment model to separate ligand

Received Apr. 5, 1994; revision accepted Aug. 1, 1994.
For correspondence or reprints contact: Philippe Millet, CERMEP, 59, Boulevard Pinel 69003 Lyon, France.

transport rate from the binding reaction. Pixel-by-pixel analyses have been developed to yield functional images of the transport rate (k_1) and the apparent distribution volume of the ligand (DV^*), thus providing independent estimates of the ligand delivery and the benzodiazepine binding (4,6,7).

The two methods are simple and need only a single injection of tracer. They can, however, only provide indices of receptor concentration, since the quantification of both receptor density (B'_{max}) and the apparent equilibrium dissociation constant ($K_d V_R$) requires different concentrations of bound ligand usually obtained using at least two injections of the ligand with different specific radioactivities. The study of Blomqvist et al. (8) was the first attempt to determine a benzodiazepine receptor map using data from two experiments on the same subject (two single radioligand injections with high- and low-specific activity, respectively). The estimation of the three parameters (receptor concentration, association and dissociation rate constants) was obtained with a kinetic approach in which the free radioligand concentration was estimated from a reference region assumed to be free of specific receptor sites.

Previous studies have shown that the five parameters of the flumazenil-benzodiazepine model can be identified with reasonable standard errors, using a multi-injection protocol (9). We have applied this modeling approach to obtain brain maps of receptor concentration, ligand affinity and the two kinetic parameters describing the exchanges between plasma and the free ligand compartments. In this article, we discuss some correlations between the model parameters, such as linear correlation between receptor density and apparent ligand affinity, which confirms results reported from several other groups, including Delforge et al. (10). Our experimental data have also been used to compute indices according to previously published methods (delayed activity maps and the distribution volume approach). The correlation between these indices and receptor concentrations identified with the multi-injection approach are discussed.

METHODS

Ligand-Receptor Model

The compartment model used in this study (Fig. 1) is a non-equilibrium, nonlinear model (9,11), which comprises three compartments (unmetabolized FMZ in plasma, free ligand and ligand bound to receptor sites) and five parameters. The parameters k_1 and k_2 are associated with the exchanges between the plasma and the free ligand compartment, B'_{max} represents the concentration of receptors available for binding, k_{on} and k_{off} are the association and dissociation rate constants, respectively, and V_R is the volume of reaction that accounts for tissue inhomogeneity (12). The parameters, k_{on} and V_R , however, cannot be estimated separately, and only the ratio k_{on}/V_R is identifiable. Consequently, only the apparent equilibrium dissociation constant $K_d V_R$ can be estimated, K_d being defined as the ratio k_{off}/k_{on} . The parameter F_v represents the fraction of blood present in the tissue volume and is assumed to be 0.04 in this study. This model does not include

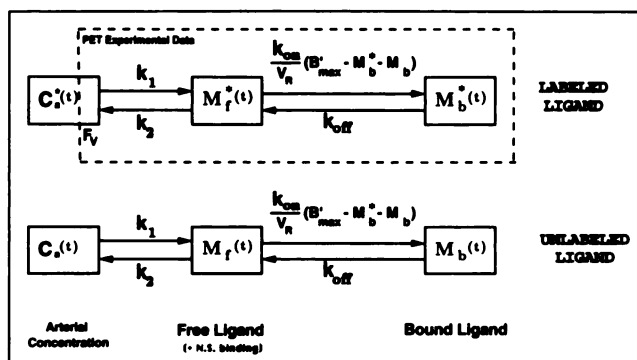


FIGURE 1. Three-compartment ligand-receptor model. (Top) Radioligand kinetics (quantities denoted with a star superscript). (Bottom) Same model for the unlabeled ligand. All ligand transfer probabilities between compartments are linear except the binding probability, which depends on the bimolecular association rate constant (k_{on}), on the local free ligand concentration ($M_f(t)/V_R$) and on the local concentration of free receptor sites [$B'_{max} - M_b^*(t) - M_b(t)$]. The PET experimental data correspond to the sum of the labeled ligand in the free and bound compartments and fraction F_v of the blood compartment assumed to be equal to 0.04.

nonspecific FMZ binding, which can be considered as negligible in vivo (13). Moreover, if a weak nonspecific binding exists, it is combined with the free ligand compartment (14,15).

The multi-injection protocols include injection of unlabeled ligand (with or without simultaneous labeled ligand injection). The kinetics of the unlabeled ligand affect the local concentration of free receptor sites and must therefore be taken into account. The unlabeled and labeled ligand kinetics are assumed to be similar, therefore, the model contains two parts with the same structure and the same parameters. The plasma concentration of the unmetabolized unlabeled ligand has been simulated from the curve corresponding to the labeled ligand. Parameter identification and simulations of labeled and unlabeled ligand kinetics have been performed using the equation system corresponding to the model diagram of Figure 1 (9).

Experimental Protocol

The parametric imaging technique was tested on experimental data obtained from three healthy male volunteers using a three-injection protocol: tracer injection, unlabeled FMZ injection and coinjection of labeled and unlabeled FMZ. FMZ was labeled with ^{11}C , using the methylation process described by Mazière et al. (16). At the start of the experiment, about 15 mCi of [^{11}C]FMZ were intravenously injected over a 1-min period. The corresponding doses of radioactive tracer were 7.0, 5.7 and 11.2 μ g, respectively. At 39 min, an intravenous injection of 0.01 mg/kg of unlabeled ligand was administered (displacement injection). At 69 min, a mixture of labeled (~ 9 mCi at the injection time) and unlabeled FMZ in the same syringe (coinjection) was injected. The injected doses were 14.2, 33.3 and 38.4 μ g, respectively, for [^{11}C]FMZ and 1.4, 6.5 and 7.5 mg, respectively, for FMZ. At time 0, the specific activity of [^{11}C]FMZ was 683, 649 and 462 mCi/ μ mole, respectively. The total experiment lasted about 120 min.

PET Measurements and Model Input Function

The PET studies were performed on an ECAT 953B positron tomograph, a brain imaging system capable of acquiring 31 continuous slices simultaneously (17). Axial resolution is 5 mm (FWHM), and spatial transverse resolution on the reconstructed

images with the Hanning filter is 8.4 mm. After each injection of labeled FMZ, 50 sequential PET scans of increasing duration (from 30 sec to 5 min) were reconstructed.

Seventy arterial blood samples (~0.3 ml each) were collected from the radial artery. The time interval between each sample varied from 5 sec, during the 2 min following each injection of labeled FMZ, to 10 min, when the change in the blood radioactivity concentration slowed down. After rapid blood centrifugation, the plasma ^{11}C radioactivity was measured using a gamma counting system. The time-activity curves were then corrected for physical decay of ^{11}C activity, and the plasma radioactivity concentrations were transformed in FMZ time-concentration curves using the corresponding specific radioactivity of [^{11}C]FMZ. The percentage of nonmetabolized [^{11}C]FMZ in plasma was measured at five different moments (2, 5, 10, 20, 39 min) by thin-layer chromatography (18) and described by the curve

$$f(t) = A + (100 - A)e^{-Bt},$$

where t is the time expressed in minutes. The mean coefficients, ($A = 31 \pm 13$, $B = 0.12 \pm 0.01$), were closely approximated to the results obtained by Debruyne et al. (19).

Parametric Imaging

For parametric imaging using the multi-injection approach, a sampling procedure for each sequential scan is necessary to access radioligand concentration versus time in all regions of the brain slice. These ROIs are composed of a set of 4 (2×2) or 12 (3×4) pixels.

The 4- and 12-pixel sampling procedures were used to build parameter maps and study correlations of the different parameters. These sampling procedures created files with all kinetic curves and information necessary for the identification procedure. To avoid biases on the brain boundaries, only ROIs where pixels were in the brain tissue were considered, using a threshold method. The model parameters were identified through a minimization of a weighted least squares cost function using a Marquardt algorithm (20). On a SparcStation 10 M30 (Sun Micro Systems, Mountain View, CA), calculation time for each slice lasted from 20 hr (for the 12-pixel sampling, which led to about 320 ROIs) to 60 hr (for the 4-pixel sampling, which led to about 1000 ROIs), corresponding to a fit of four parameters from a 120-min experiment. The fitting procedures provided a file of estimated parameters from which maps were built.

The first part of our experiment data, equivalent to that of a single-tracer injection study, was used to test simplified methods (distribution volume approach and delayed activity maps). Parametric images thus were obtained using the two-parameter, two-compartment model (4) and 4-pixel sampling. The two parameters, denoted by k_1 and k_2' , were identified by the Marquardt minimization method with a vascular fraction, F_v , assumed to be equal to 0.04, and the unmetabolized FMZ concentration in plasma as the input function. Images of parameter k_1 and of k_1/k_2' (the apparent distribution volume denoted by DV^*) were constructed. Early and delayed activity images were reconstructed during the first 3 min and between 24 and 39 min, respectively, after injection of high-specific activity FMZ.

RESULTS

Parameter Identification

Fitting the five-parameter three-compartment model to time-concentration curves from our experimental protocol

provided estimates for kinetic rate constants and receptor densities with acceptable standard errors, even in low receptor density areas (9). These studies, however, were performed with a limited number of large ROIs.

Parametric imaging requires small ROIs to obtain images with good resolution. Some of these regions have a low concentration of receptor sites, and the binding parameters were difficult to estimate. Therefore, difficulties in fitting the five parameters of the model due to the noise level of small and receptor-poor regions were not surprising initially. We then investigated the possibility of improving parametric estimation by reducing the number of parameters. Previous results showed that the dissociation rate constant k_{off} is independent of receptor concentration and can be considered a constant independent of the ROIs (9). Therefore, for each subject, the parameters k_{off} were fixed to the value estimated from a fitting procedure of the whole-brain region time-activity curve.

To check that this simplification does not affect the results, we compared the estimates obtained with the four- and the five-parameter models in receptor-poor and receptor-rich regions. Table 1 shows the parameter estimates for four ROIs and the standard errors calculated using the covariance matrix. In receptor-rich regions, the fitting procedure provides similar estimates, regardless of the model used, with better standard errors. For the four-parameter model, however, the standard error on parameter k_{on}/V_R was reduced by a factor of ~10. The main parameters (B'_{max} and $K_d V_R$) remain unchanged by this simplification, with variations smaller than 1%. In receptor-poor regions, the fitting procedure with the five-parameter model results in unacceptable standard errors for parameters k_{on}/V_R and k_{off} (e.g., in Table 1: 0.207 ± 0.411 and 0.112 ± 0.204 ml/[pmole min], 1.41 ± 5.03 and 0.64 ± 0.75 min $^{-1}$, respectively). The use of the four-parameter model (k_{off} fixed), dramatically reduces the standard errors on k_{on}/V_R (0.108 ± 0.024 and 0.131 ± 0.041 ml/[pmole min]) without altering the order of magnitude of the other values.

The decrease in the number of pixels in the small ROIs increases noise in the time-concentration curves. Consequently, a balance between these two factors (sampling and noise) must be found. Parameter estimates have been studied in receptor-poor and receptor-rich regions with 4-pixel and 12-pixel sampling. Four-pixel sampling produces noisier experimental data and, consequently, a higher standard error for each parameter is expected. The estimated parameters with 4-pixel sampling (means and standard errors) appear to be similar to those with 12-pixel sampling, despite increasing noise. Studies using ROIs with a smaller number of pixels (1 or 2 pixels) led to unacceptable results due to a significant amount of noise.

The diagram in Figure 2 represents the number of 4-pixel ROIs as a function of the relative standard errors for the B'_{max} parameter. The standard errors were calculated with a covariance matrix. The relative standard errors are less than 20% in about 75% of the ROIs. In a small number of ROIs (less than 1%), this error estimate is large (more than

TABLE 1

Model Parameters of the FMZ Kinetics Estimated from Four Regions of Interest with the Five-Parameter, Three-Compartment Model and the Four-Parameter, Three-Compartment Model

Parameters (units)	Parameter estimates (\pm s.e. [*])							
	Receptor-rich regions [†]				Receptor-poor regions [‡]			
	Region 1		Region 2		Region 3		Region 4	
	Five parameters	Four parameters	Five parameters	Four parameters	Five parameters	Four parameters	Five parameters	Four parameters
B'_{max} (pmole/ml)	71.5 \pm 5.9	71.3 \pm 3.5	54.0 \pm 4.1	54.9 \pm 3.2	21.6 \pm 7.4	22.2 \pm 4.9	15.1 \pm 7.0	15.8 \pm 5.9
k_1 (min^{-1})	0.30 \pm 0.02	0.34 \pm 0.02	0.27 \pm 0.01	0.27 \pm 0.01	0.15 \pm 0.02	0.16 \pm 0.02	0.13 \pm 0.02	0.14 \pm 0.02
k_2 (min^{-1})	0.51 \pm 0.04	0.55 \pm 0.04	0.49 \pm 0.05	0.50 \pm 0.04	0.27 \pm 0.04	0.26 \pm 0.03	0.31 \pm 0.05	0.32 \pm 0.05
k_{on}/V_R (ml/[pmole min])	0.075 \pm 0.043	0.066 \pm 0.004	0.081 \pm 0.042	0.080 \pm 0.003	0.207 \pm 0.411	0.108 \pm 0.024	0.112 \pm 0.204	0.131 \pm 0.041
k_{off} (min^{-1})	0.88 \pm 0.52	0.756 [§]	0.74 \pm 0.47	0.756 [§]	1.41 \pm 5.03	0.756 [§]	0.64 \pm 0.75	0.756 [§]
$K_d V_R^*$ (pmole/ml)	11.7 \pm 1.3	11.5 \pm 0.7	9.1 \pm 0.7	9.4 \pm 0.4	6.8 \pm 1.6	7.0 \pm 1.5	5.7 \pm 4.2	5.8 \pm 1.8

^{*}Standard errors corresponding to the parameter estimates calculated by using the covariance matrix.
^{**} $K_d = k_{off}/k_{on}$.
[§]Fixed parameter.
[†]Cortical regions.
[‡]Cerebellar regions.

60%) but only because the large residual distance between noisy experimental data and the simulated curves, the fitting result and the order of magnitude of the parameter values appear valid. The same results were found for the $K_d V_R$ parameter.

Brain Maps of Model Parameters

From the three-injection protocol data, all model parameters (k_{off} being fixed) were estimated and parametric images of receptor density (B'_{max}) and three kinetic parameters (k_1 , k_2 , k_{on}/V_R) were built. The $K_d V_R$ image was

computed by dividing the dissociation rate constant (k_{off}) by the k_{on}/V_R image.

For example, Figure 3 shows the parametric images of B'_{max} , $K_d V_R$, k_1 , k_2 in the brain of a normal volunteer. The images represent one tomographic slice passing through

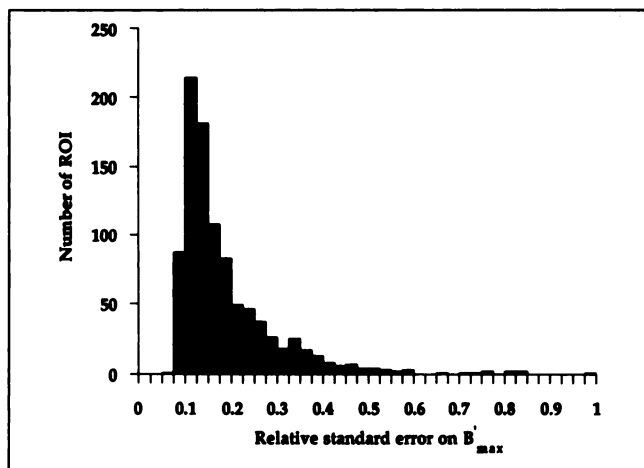


FIGURE 2. Diagram representing the number of 4-pixel ROIs as a function of the corresponding relative standard errors on B'_{max} . These results correspond to the parametric images obtained with our three-injection protocol shown in Figure 3.

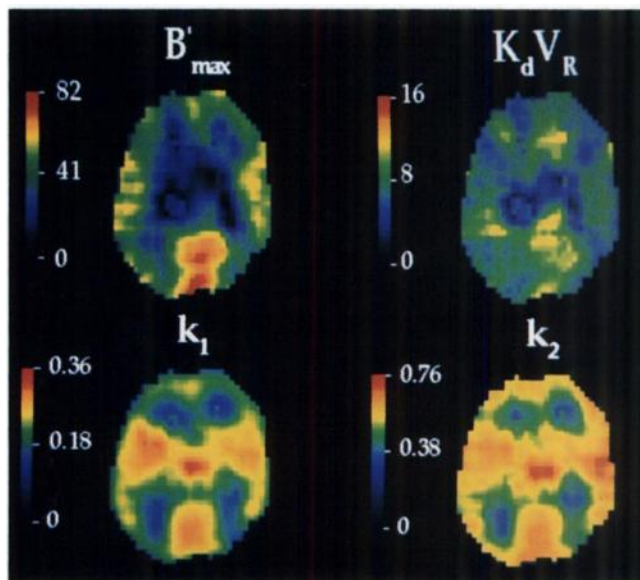


FIGURE 3. Parametric images of B'_{max} (pmole/ml), $K_d V_R$ (pmole/ml), k_1 (min^{-1}) and k_2 (min^{-1}) corresponding to a normal brain slice and estimated by the three-injection protocol. The tomographic slice passes through the basal ganglia, the thalamus and the frontal, temporal and occipital cortices. Four-pixel sampling allows good definition for each parametric image.

the basal ganglia, thalamus and the frontal, temporal and occipital cortices. The B'_{max} values reveal a relatively homogeneous pattern across the major gray matter structures, with lower values observed in white matter, resulting in good structural definition of the B'_{max} image (Fig. 3, top left). The k_2 map appears to correlate with the k_1 map, which represents the [^{11}C]FMZ transport rate (Fig. 3, bottom right). Large variations (range 4 to 14 pmole/ml) are observed in the $K_d V_R$ map (Fig. 3, top right).

Correlations between Parameters

Parametric images provide several estimated values that correspond to the large volume of ROIs, thus allowing study of the correlations between the model parameters. In a recent study using large ROIs in several subjects, linear correlation was shown between receptor density (B'_{max}) and the apparent equilibrium dissociation rate constant ($K_d V_R$) (10). This correlation clearly appears again in Figure 4A, which represents the plot of $K_d V_R$ (computed using a fixed k_{off} and estimated k_{on}/V_R) and the estimated B'_{max} values across all regions of the slice represented in Figure 3. The solid straight line corresponds to the linear correlation given by the equation:

$$K_d V_R = C_1 + C_2 B'_{max},$$

which seems to be significant ($r = 0.83$). Figure 4B shows the relationship between B'_{max} and k_{on}/V_R . Since k_{off} is assumed to be a constant (0.756 min^{-1} in this example) independent of the ROIs, k_{on}/V_R is directly related to $K_d V_R$, and thus the analytical relationship between the association rate constant (k_{on}/V_R) and receptor density (B'_{max}) can be deduced from the previous correlation shown in Figure 4A between $K_d V_R$ and B'_{max} . The following equation is then obtained:

$$\frac{k_{on}}{V_R} = \frac{k_{off}}{(C_1 + C_2 B'_{max})}$$

This curve, plotted in Figure 4B (solid line), correlates effectively with the estimated values ($r = 0.79$).

The $k_1:k_2$ ratio is often considered as a constant independent of the ROIs; these two parameters are assumed to depend on blood flow (4,21,22). We studied the $k_1:k_2$ ratio as a function of B'_{max} values (Table 2). This result does not show any correlation between the two parameters ($r = 0.01$) and indicates a variability independent of the B'_{max} value ($k_1/k_2 = 0.555 \pm 0.056$).

Table 2 gives the detailed data for all three experiments, while Figures 1–7 refer only to experiment 3.

Activity Maps and Two-Compartment Approaches

Several authors have proposed using delayed activity images as an index of receptor density and early activity images as an index of ligand transport rate (23–25). Figure 5 shows a delayed activity image (top left) corresponding to the activity measured with PET between 24 and 39 min after tracer injection, and an early activity

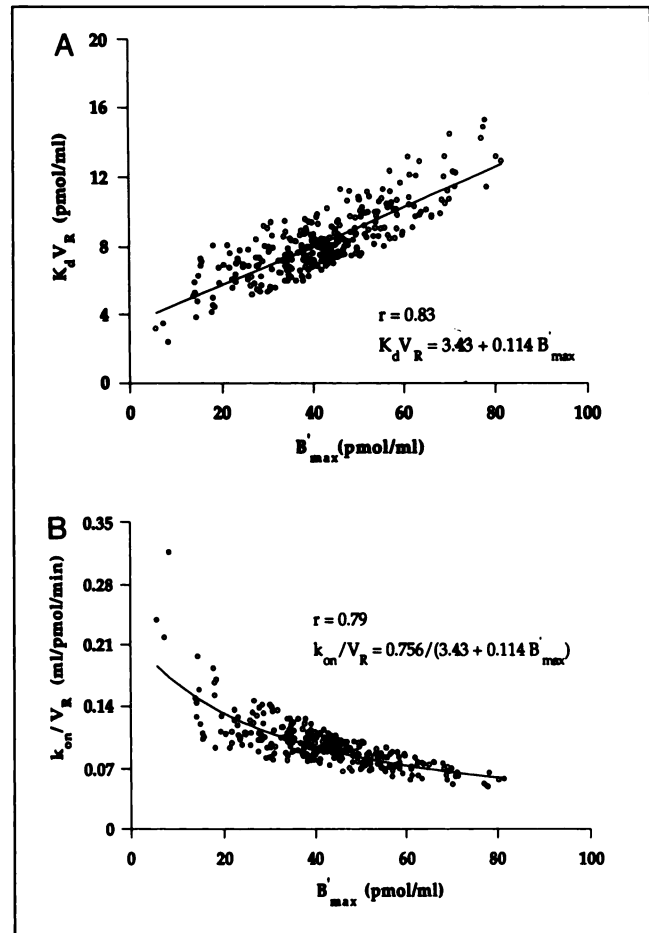


FIGURE 4. Estimated values of $K_d V_R$ (A) and of k_{on}/V_R (B) as a function of the B'_{max} estimates. The open circles are estimated parameter values obtained from all regions of the same brain slice (Fig. 3). The solid line in Figure 4A represents the linear correlation ($r = 0.83$). The nonlinear curve presented in Figure 4B is deduced from this previous correlation and the k_{off} value (0.756 min^{-1}).

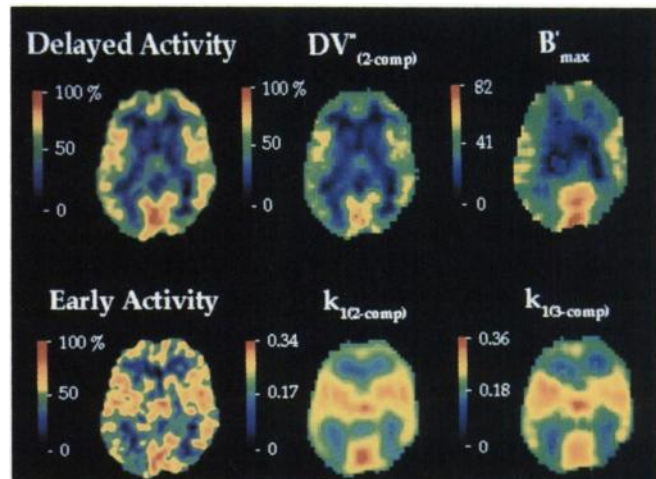


FIGURE 5. Delayed and early activity images (first column) of the apparent distribution volume and k_1 from the two-compartment model (second column) and of B'_{max} and k_1 from the three-compartment model (third column). It represents the same slice in Figure 3. The first row shows three indices of the receptor density; second row represents three indices of the ligand transport rate.

TABLE 2
Detailed Results of Correlations for Three Volunteers

Correlations	Exp. 1	Exp. 2	Exp. 3	Mean ± s.d. ^{††}
$k_{\text{off}} V_R = C_1 + C_2 B'_{\text{max}}$	$C_1 = 3.19$ $C_2 = 0.122$ $r = 0.83$	$C_1 = 5.38$ $C_2 = 0.084$ $r = 0.77$	$C_1 = 3.43$ $C_2 = 0.114$ $r = 0.83$	$r = 0.81 \pm 0.03$
$k_{\text{on}} V_R = k_{\text{off}} / (C_1 + C_2 B'_{\text{max}})$	$k_{\text{off}} = 0.722$ $r = 0.81$	$k_{\text{off}} = 0.394$ $r = 0.70$	$k_{\text{off}} = 0.756$ $r = 0.79$	$r = 0.77 \pm 0.05$
$k_1/k_2 = C_3 + C_4 B'_{\text{max}}$	$C_3 = 0.411$ $C_4 = 0.00066$ $r = 0.15$	$C_3 = 0.630$ $C_4 = -0.00025$ $r = 0.09$	$C_3 = 0.555$ $C_4 = 0.00042$ $r = 0.01$	$r = 0.08 \pm 0.06$
$D_{\text{act.}}^{\ddagger} = C_5 + C_6 DV''_{\text{exp.}}$	$C_5 = 2.92$ $C_6 = 26.8$ $r = 0.991$	$C_5 = -4.26$ $C_6 = 16.7$ $r = 0.989$	$C_5 = 4.60$ $C_6 = 17.9$ $r = 0.996$	$r = 0.992 \pm 0.003$
$E_{\text{act.}}^{\ddagger\ddagger} = C_7 + C_8 k_1$	$C_7 = 5.66$ $C_8 = 260.5$ $r = 0.933$	$C_7 = 10.50$ $C_8 = 175.5$ $r = 0.907$	$C_7 = 2.88$ $C_8 = 267.0$ $r = 0.930$	$r = 0.92 \pm 0.01$
$DV''_{\text{exp.}}^{\ddagger} = C_9 + C_{10} B'_{\text{max}}$	$C_9 = 1.18$ $C_{10} = 0.035$ $r = 0.800$	$C_9 = 1.78$ $C_{10} = 0.039$ $r = 0.824$	$C_9 = 1.88$ $C_{10} = 0.033$ $r = 0.691$	$r = 0.77 \pm 0.06$
$DV''_{\text{the.}}^{\ddagger} = C_3 (1 + B'_{\text{max}} / (C_1 + C_2 B'_{\text{max}}))$	$r = 0.811$	$r = 0.815$	$r = 0.717$	$r = 0.78 \pm 0.05$
$DV''_{\text{the.}}^{\S} = C_{11} (1 + B'_{\text{max}} / (C_{12} + C_{13} B'_{\text{max}}))$	$C_{11} = 0.581$ $C_{12} = 5.54$ $C_{13} = 0.143$ $r = 0.812$	$C_{11} = 0.795$ $C_{12} = 7.69$ $C_{13} = 0.101$ $r = 0.825$	$C_{11} = 0.553$ $C_{12} = 3.89$ $C_{13} = 0.105$ $r = 0.722$	$r = 0.79 \pm 0.05$
No. of values	314	302	335	

* k_{off} fixed to a value estimated from a fitting procedure of the whole-brain region time-activity curve.

† DV'' estimated with a two-parameter, two-compartment model.

‡ DV'' calculated with Equation 2.

§ DV'' fitted using a Marquardt algorithm.

‡Activity measured with PET between 24 and 39 min postinjection.

‡‡Activity measured with PET during the first 3 min after the tracer injection.

††Mean correlation coefficient (r) ± s.d.

image (bottom left) corresponding to PET activity measured during the first 3 min after tracer injection.

Koeppel et al. (4) have proposed the use of a two-compartment model, including two parameters that can be estimated from a single tracer injection protocol. This configuration adequately describes the kinetic behavior of [¹¹C]flumazenil in the human brain. Due to the reduced number of parameters, the two parametric images associated to k_1 and DV'' were obtained easily (see Fig. 5, middle images).

In Figure 6A, the delayed activities are plotted (normalized to the maximum activity) versus the corresponding DV'' estimates obtained by the Koeppel approach. The linear correlation is strong ($r = 0.996$ for this example, and $r = 0.992 \pm 0.003$ for the three volunteers; see Table 2). Similarly, the early activity and k_1 estimated with the two-compartment model are compared (Table 2). This correlation is significant ($r = 0.93$) but not as strong as the former. This is not surprising since the simulations showed that the binding is rapid and has a significant effect on PET tracer concentration even during the first 3 min (9).

Comparison between Two- and Three-Compartment Approaches

Since the apparent distribution volume is related to the binding effect, Koeppel et al. (4) suggested that this combined parameter can be used as an index of receptor density. If the system is assumed to be in an equilibrium state, DV'' is related to receptor density (B'_{max}) and to the kinetic

parameters of the three-compartment model by the following equation:

$$DV'' = \frac{k_1}{k_2} \left(1 + \frac{B'_{\text{max}} k_{\text{on}}}{k_{\text{off}} V_R} \right). \quad \text{Eq. 1}$$

To test the validity of this equation, the apparent distribution volume was calculated with both methods: First, this parameter was computed from the ratio of k_1 and k_2 estimates obtained with the two-compartment model; second, it was estimated using Equation 1 and the parameters obtained with the three-compartment model. For the bi-compartmental approach, only the first 39 min of experimental data were used, which corresponds to the single-tracer injection experiment. The relationship between these two estimates is shown in Figure 6B. The correlation coefficient across all regions is 0.989 and the two DV'' estimates are almost identical ($DV''_{(2\text{-comp})} = 0.005 + 0.971 DV''_{(3\text{-comp})}$).

The apparent distribution volume DV'' is assumed to be an index of receptor binding. A comparison between the apparent distribution volume image (first row, middle) and the B'_{max} image (first row, right side) is shown in Figure 5. The global DV'' and B'_{max} maps have similar profiles, even though they do not look strictly equivalent in all brain regions. The correlation between these two parameters can be studied ROI-by-ROI using the graph shown in Figure 7. These two approaches, however, result in two different correlations. With the two-compartment approach, the dis-

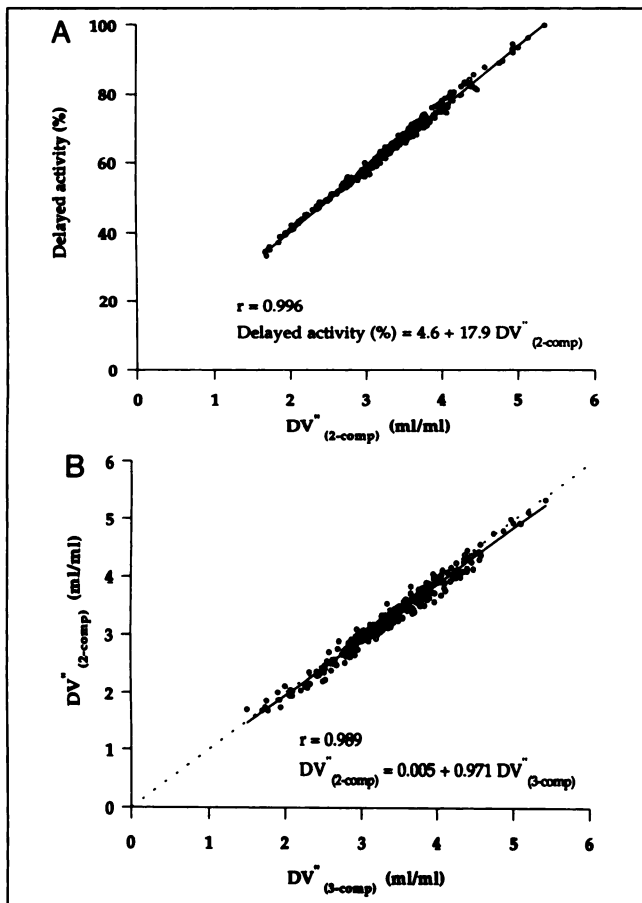


FIGURE 6. Relationship between the delayed activity map and B'_{max} . (A) Comparison of the apparent distribution volume from the two-compartment model with the corresponding parameters estimated by the three-compartment model (B). The solid lines represent the linear relations. The linear correlation corresponding to the Figure 6B ($r = 0.989$) is very close to the identity equation (dotted lines).

tribution volume is a linear index of the receptor concentration only if it is assumed that k_1/k_2 and $K_d V_R$ are constants independent of the ROIs (see Equation 1): the linear correlation was tested and the coefficient correlation (0.691) is reasonable ($DV'' = C_9 + C_{10} B'_{max}$, long-dashed line in Figure 7, $C_9 = 1.88$, $C_{10} = 0.033$; Table 2). Data obtained with the three-compartment approach support our view of a constant value independent of B'_{max} for k_1/k_2 (see Table 2), but $K_d V_R$ cannot be considered a constant since we observed a linear relation between $K_d V_R$ and B'_{max} (Fig. 4A). This leads to the following nonlinear relationship:

$$DV'' = \frac{k_1}{k_2} \left(1 + \frac{B'_{max}}{C_1 + C_2 B'_{max}} \right), \quad \text{Eq. 2}$$

where k_1/k_2 , C_1 and C_2 are equal to 0.555, 3.43 and 0.114, respectively, in our example (Fig. 4A and Table 2). This equation was plotted (solid line in Fig. 7). The coefficient correlation (0.717) is better than that obtained with the linear regression line. Equation 2 also was fitted to data

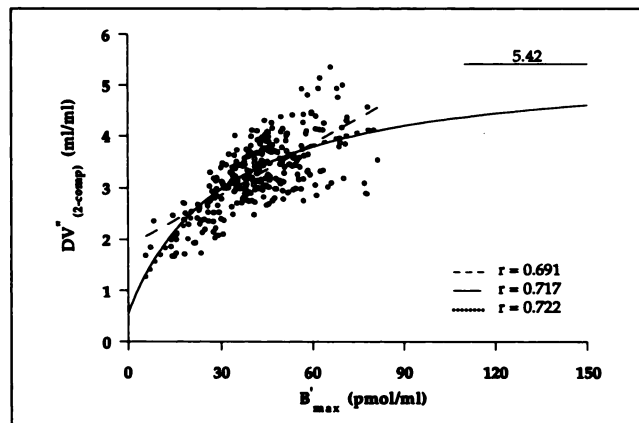


FIGURE 7. Relationship between the apparent distribution volume (DV'') and receptor concentration (B'_{max}). The long dashed line represents the linear correlation ($r = 0.691$). The solid line is plotted using Equation 2 and fixed coefficients C_1 and C_2 deduced from the correlation shown in Figure 4A ($C_1 = 3.43$, $C_2 = 0.114$). When B'_{max} increases indefinitely, DV'' is an asymptotic value equal to 5.42. The dotted line represents the curve obtained by fitting Equation 2 to all DV'' values: $DV'' = 0.553 (1 + B'_{max}/(3.89 + 0.105 B'_{max}))$, ($r = 0.722$).

using a direct least squares method. The result, $DV'' = 0.553 [1 + B'_{max}/(3.89 + 0.105 B'_{max})]$, represented by a dotted line in Figure 7, approximates the nonlinear correlation previously described (solid line) and corresponds to a slightly better correlation coefficient (0.722). Similar results were obtained for the other two volunteers (Table 2).

When k_1 is estimated with the two-compartment model, it is assumed to be the same parameter obtained with the three-compartment model (4). Linear correlation between the two k_1 estimates shows a good correlation coefficient ($k_{1(2-comp)} = 0.03 + 0.81 k_{1(3-comp)}$, $r = 0.93$, not shown), but this correlation is significantly different to the identity relation, since the k_1 values obtained with the two-compartment model are 5%–15% smaller than the values obtained with the three-compartment model.

DISCUSSION

Parameter Values

The aim of parametric imaging is to provide all parameters with maps combining high definition and valid results. The former objective requires small ROIs and the latter requires acceptable standard deviations. The use of small ROIs with a weak signal (in receptor-poor regions) leads to noisy time-concentration curves and difficulties in identifying all model parameters. Two solutions are available to overcome these problems: filtering the time-concentration curves or decreasing the number of model parameters.

A decrease in parameters implies knowing either the value of some parameters or the correlations between them. During our first attempt, the $k_1:k_2$ ratio was assumed to be constant, independent of ROIs and estimated with values of k_1 and k_2 obtained from the whole-brain region. This assumption is used by some authors (21,26) and is justified by the independence between $k_1:k_2$ and the recep-

tor concentration (Table 2). This constraint does not improve results due to numerical difficulties in estimating binding reaction parameters in receptor-poor regions. In such regions, instantaneous decrease of the curve slope (displacement experiment) is not easily detected in receptor-poor regions, because of the experimental uncertainties that may cover up the small level of displacement [see an example of curves in Delforge et al. (27)]. It is well known, however, that the parameter k_{off} determines the slope of the PET time-concentration curve after the displacement time and that, conversely, this parameter is mainly identified from this slope (27). Consequently, if this slope is not clearly visible, the estimate of the dissociation constant may be meaningless, since this value is usually overestimated with a large standard deviation. We found that this overestimation is compensated by a similar increase in the k_{on}/V_R parameter, which in fact leads to a $K_d V_R$ estimate with a correct order of magnitude but with a large standard deviation.

Spatial sampling of PET images is an important step. The best solution is a pixel-by-pixel study, but physical limitations such as noise or PET resolution does not allow this. We did, however, test several sampling grids. Twelve-pixel sampling was chosen as a reference model and compared to 4-pixel sampling, which provides higher standard errors but produces a similar image pattern with better resolution. Increasing the image sampling (1 and 2 pixels) provides aberrant values. Consequently, a 4-pixel sampling was selected because it leads to good parametric image definition with reliable values.

Finally, even for small ROIs, B'_{max} and $K_d V_R$ were of the same order of magnitude as those cited by Delforge et al. (9). Because of the constraint on parameter k_{off} , standard errors calculated for each parameter, using the covariance matrix (Fig. 2), were not much larger than those found by Delforge et al. (9) despite small ROI size.

Parametric Imaging

The use of a three-compartment model with a multi-injection protocol allows the study of neuroreceptor distribution in the living brain with parametric imaging (B'_{max} and $K_d V_R$ images; see Fig. 3). The decrease in the number of model parameters by fixing the dissociation rate constant (k_{off}) has clearly solved many problems in the fitting procedure and the images without causing artifacts. This multi-injection method is adaptable for brain imaging and results in nonaberrant values, such as the negative ones obtained, for example, by Blomqvist et al. (8) and Lammertsma et al. (26). The calculation time, however, is a drawback.

Several parameter sets are obtainable with parametric imaging, which allows the study of the relation between model parameters on a large number and range of values. Some joint results were predictable, such as the correlation between the equilibrium dissociation constant $K_d V_R$ and the concentration of receptor sites B'_{max} , as reported by Delforge et al. (10). The example shown in Figure 4A

confirms this result on several parameter values and for a wide range of receptor concentrations. Since the dissociation rate constant (k_{off}) is set up, the linearity between $K_d V_R$ and B'_{max} corresponds to a nonlinear correlation between the association rate constant (k_{on}/V_R) and the concentration of receptor sites (B'_{max}) as shown in Figure 4B. These results agree with those of Delforge et al. (10), who obtained them without hypothesizing about dissociation rate constants.

Study of Distribution Volume

The multi-injection approach is a complicated method that is difficult to apply to human studies. Therefore, simpler methods applicable in routine patient examinations are needed. Koeppe et al. (4) have estimated apparent distribution volume, which is considered an index of the receptor density. All simplified approaches, however, are based on hypotheses that need verification. For the two-compartment approach, only the first 39 min of experimental data were used, which corresponds to the single tracer injection experiment. This duration is sufficient for reliable estimation of k_1 and DV'' , since the estimates of the two parameters (values and variances) become stable within 20–30 min of data acquisition.

The two-compartment model used in the distribution volume approach is deduced from the usual three-compartment model, assuming that all tissue compartments are in an equilibrium state and therefore the free and bound ligand compartments can be lumped together in a single tissue compartment. These hypotheses result in the equivalence of the k_1 parameters in the two models and in Equation 1 giving the apparent distribution volume DV'' from the three-compartment model parameters. The correlations we obtained ($r = 0.989$ and 0.93 , respectively) validate this simplified model. The significant underestimation (from 5% to 15%) of k_1 by the two-compartment model is probably the consequence of the time (5–10 min) necessary for the system to reach equilibrium (9). This explanation is supported by the fact that this underestimation appears smaller in the receptor-poor regions in which equilibrium is reached more rapidly.

Figure 6A shows close correlation between delayed activity and the distribution volume. This result is also very clear in the images published by Frey et al. (6). In fact, this correlation is easily explained by the theory. The distribution volume concept assumes that equilibrium is reached between the three model compartments. In which case, use of the model equations during equilibrium results in the following relationship:

$$DA(t) = \lambda C_a(t) \left[F_V + \frac{k_1}{k_2} \left(1 + \frac{B'_{max} k_{on}}{k_{off} V_R} \right) \right] \\ = \lambda C_a(t) [F_V + DV''], \quad \text{Eq. 3}$$

where $DA(t)$ is the delayed activity, λ is the constant and $C_a(t)$ is the input function.

The main advantage of the delayed activity method is

that blood sampling is not needed. Delayed activity images provide similar results to distribution volume images ($r = 0.996$ in Figure 6A), but the early images are of poorer quality to estimate k_1 ($r = 0.93$).

An advantage of the DV'' images is that they provide absolute values (because of use of the input function) and allow intersubject and intergroup comparisons, whereas delayed images correspond only to relative indices of receptor density. Normalization of these activity images is possible, for example, by dividing the count number by the injected dose.

The second step is validation of the use of the distribution volume as an index of receptor density. A linear correlation between DV'' and B'_{\max} is based on the assumption that k_1/k_2 and $K_d V_R$ are independent of ROIs (Eq. 1). We used $k_1:k_2$ ratio as a constant, despite large variability compared to B'_{\max} values (Table 2). We found, however, that $K_d V_R$ is linearly correlated with B'_{\max} . Substituting $K_d V_R$ from this correlation into Equation 1 gives DV'' and yields a nonlinear relationship (Eq. 2). This last equation gives a correlation coefficient only slightly better than that obtained with the linear relation between B'_{\max} and DV'' . The two correlations between DV'' and B'_{\max} are not contradictory if one considers only the usual range of B'_{\max} values in the human brain (from 5 to 100 pmole/ml). Consequently, the linear correlation is acceptable, although nonlinearity was proven by the experimental results showed in Figure 4A.

This approximation, however, appears invalid for receptor concentrations higher than 100 pmole/ml since the curve associated with nonlinear correlation tends to a plateau at a level given by $(k_1/k_2)(1 + 1/\alpha)$ (deduced from Eq. 2). In our example ($k_1/k_2 = 0.555$, $\alpha = 0.114$), this level (5.42) does not reach a B'_{\max} value equal to 150 pmole/ml (Fig. 7). This discussion is valid for the two other examples given in Table 2. The mean correlation coefficients in the three experiments are 0.77 ± 0.06 and 0.78 ± 0.05 for the linear and nonlinear correlations, respectively (Table 2).

We do not exclude that, with other molecules or in some patient studies, the estimated B'_{\max} values correspond to the part of the curve with a low slope. In such a case, a variation of the B'_{\max} value will not significantly modify the distribution volume, and one could no longer consider it a good index of receptor concentration.

CONCLUSION

This study shows the possibility of obtaining parametric images corresponding to flumazenil-benzodiazepine model parameters from data acquired after a single-experiment multi-injection protocol. The complexity of this protocol (the need of three injections, a 2-hr experiment, blood sampling and a metabolite study) and the long duration for the calculations, make this approach difficult to apply in routine examination. This method can be considered a reference protocol to validate other simplified approaches.

We found a close correlation between the delayed activity images and the apparent distribution volume images which was justified by the equilibrium state between the three model compartments. Therefore, the delayed FMZ images can be considered as good an index of benzodiazepine receptor concentration as apparent distribution volume.

The linear relationship between B'_{\max} and $K_d V_R$ observed experimentally results in nonlinear correlation between B'_{\max} and DV'' . With the range of benzodiazepine receptor densities observed in human studies, however, the nonlinear correlation coefficient is higher but does not differ from the linear one. In spite of a non-negligible variability, we believe that the distribution volume and delayed activity images approaches are valid with FMZ.

The use of these approaches with other molecules implies verifying the equilibrium state between the three model compartments after tracer injection. Equilibrium may be unattainable if the binding rate is too large in comparison to the other rate constants.

ACKNOWLEDGMENTS

The authors thank the cyclotron and radiochemistry staff of the Service Hospitalier Frédéric Joliot, M. Janier and G. De Lamery for critical review of this paper and R. Le Goff, O. Lamer and V. Brulon for their technical assistance. We also thank Hoffman La Roche laboratory for generously providing flumazenil.

REFERENCES

- Mazière M, Prenant C, Sastre J, et al. 11C-RO 15 1788 et 11C-flunitrazepam, deux coordonnés pour l'étude par tomographie par émission de positons de sites de liaison des benzodiazépines. *C R Acad Sci (Paris)* 1983;296:871-876.
- Persson A, Ehrin E, Eriksson L, et al. Imaging of [11C]-labeled RO 15-1788 binding to benzodiazepine receptors in the human brain by positron emission tomography. *J Psychiatr Res* 1985;19:609-622.
- Samson Y, Hantraye P, Baron JC, Soussaline F, Comar D, Mazière M. Kinetics and displacement of [11C]RO 15-1788, a benzodiazepine antagonist, studied in human brain in vivo by positron tomography. *Eur J Pharmacol* 1985;110:247-251.
- Koeppel RA, Holthoff VA, Frey KA, Kilbourn MR, Kuhl DE. Compartmental analysis of [11C]flumazenil kinetics for the estimation of ligand transport rate and receptor distribution using positron emission tomography. *J Cereb Blood Flow Metab* 1991;11:735-744.
- Pappata S, Samson Y, Chavoix C, Prenant C, Mazière M, Baron JC. Regional specific binding of [11C]RO 15 1788 to central type benzodiazepine receptors in human brain: quantification evaluation by PET. *J Cereb Blood Flow Metab* 1988;8:304-313.
- Frey KA, Holthoff VA, Koeppel RA, Jewett DM, Kilbourn MR, Kuhl DE. Parametric in vivo imaging of benzodiazepine receptor distribution in human brain. *Ann Neurol* 1991;30:663-672.
- Holthoff VA, Koeppel RA, Frey KA, et al. Differentiation of radioligand delivery and binding in the brain: validation of a two-compartment model for [11C]flumazenil. *J Cereb Blood Flow Metab* 1991;11:745-752.
- Blomqvist G, Pauli S, Farde L, Eriksson L, Persson A, Halldin C. Maps of receptor binding parameters in the human brain: a kinetic analysis of PET measurements. *Eur J Nucl Med* 1990;16:257-265.
- Delforge J, Syrota A, Bottlaender M, et al. Modeling analysis of [11C]flumazenil kinetics studied by PET: application to a critical study of the equilibrium approaches. *J Cereb Blood Flow Metab* 1993;13:454-468.
- Delforge J, Millet P, Pappata S, et al. Correlation between the apparent affinity and the receptor concentration in the flumazenil-benzodiazepine interaction model [Abstract]. *J Nucl Med* 1994;35:67P.
- Syrota A, Paillotin G, Davy JM, Aumont MC. Kinetics of in vivo binding of antagonist to muscarinic cholinergic receptor in the human heart studied by positron emission tomography. *Life Sci* 1984;35:937-945.

12. Delforge J, Syrota A, Bendriem B. The reaction volume: accounting for tissue heterogeneity in in vivo ligand-receptor interaction studies [Abstract]. *J Nucl Med* 1994;35:137P.
13. Goeders NE, Kuhar MJ. Benzodiazepine receptors in vivo with (³H)RO 15-1788. *Life Sci* 1985;37:345-355.
14. Mintun MA, Raichle ME, Kilbourn MR, Wooten F, Welch MJ. A quantitative model for the in vivo assessment of drug binding sites with positron emission tomography. *Ann Neurol* 1984;15:217-227.
15. Perlmutter JS, Larson KB, Raichle ME, et al. Strategies for in vivo measurement of receptor binding using positron emission tomography. *J Cereb Blood Flow Metab* 1986;6:154-169.
16. Mazière M, Hantraye P, Prenant C, Sastre J, Comar D. Synthesis of ethyl 8-fluoro-5,6-dihydro-5-(11C)methyl-6-oxo-4H-imidazo(1,5-a) benzodiazepine-3-carboxylate (RO 15-1788): a specific radioligand for in vivo study of central benzodiazepine receptors by positron emission tomography. *Int J Appl Radiat Isotop* 1984;35:973-978.
17. Bendriem B, Trebossen R, Frouin V, Lamer O, Brulon V, Syrota A. Evaluation of a PET scanner in 2D and 3D acquisition mode. In: Moucci JP, Plonsey R, Coatrieux JL, Laxminarayan S, eds. *Proceedings of the annual international conference of the IEEE Engineering in Medicine and Biology Society*. 1992;14:1837-1840.
18. Loc'h C, Hantraye P, Khalili-Varasteh M, et al. Carbon-11-flumazenil metabolism: analysis of unchanged ligand in baboon plasma. *J Nucl Med* 1990;31:897.
19. Debruyne D, Abadie P, Barre L, et al. Plasma pharmacokinetics and metabolism of the benzodiazepine antagonist ¹¹C-RO 15-1788 (flumazenil) in baboon and human during positron emission tomography studies. *Eur J Drug Metabol Pharmacol* 1991;16:141-152.
20. Marquardt DW. An algorithm for least-square estimation of non-linear parameters. *SIAM J* 1963;11:431-441.
21. Price JC, Mayberg HS, Dannals RF, et al. Measurement of benzodiazepine receptor number and affinity in humans using tracer kinetic modeling, positron emission tomography and [¹¹C]flumazenil. *J Cereb Blood Flow Metab* 1993;13:656-667.
22. Lassen N. Neuroreceptor quantitation in vivo by the steady-state principle using constant infusion or bolus injection of radioactive tracers. *J Cereb Blood Flow Metab* 1993;12:709-716.
23. Shinotoh H, Yamasaki T, Inoue O, et al. Visualization of specific binding sites of benzodiazepine in human brain. *J Nucl Med* 1986;27:1593-1599.
24. Shinotoh H, Iyo M, Yamada T, et al. Detection of benzodiazepine receptor occupancy in the human brain by positron emission tomography. *Psychopharmacol* 1989;99:202-207.
25. Sadzot B, Frost JJ. Benzodiazepine receptors. In: Frost J, Wagner H, eds. *Quantitative imaging: neuroreceptors, neurotransmitter and enzymes*. New York: Raven Press; 1990:109-127.
26. Lammerstma A, Lassen N, Prevett M, et al. Quantification of benzodiazepine receptors in vivo using ¹¹C-flumazenil: application of the steady state principle. *Ann Nucl Med* 1993;7:S32-S33.
27. Delforge J, Syrota A, Mazoyer BM. Identifiability analysis and parameter identification of an in vivo ligand-receptor model from PET data. *IEEE Trans Biomed Eng* 1990;37:653-661.